Andreev Reflection in an s-Type Superconductor Proximized 3D Topological Insulator

Tikhonov, E.S.; Shovkun, D.V.; Snelder, M.; Stehno, M.P.; Huang, Y.; Golden, M.S.; Golubov, A.A.; Brinkman, A.; Khrapai, V.S.

DOI
10.1103/PhysRevLett.117.147001

Publication date
2016

Document Version
Final published version

Published in
Physical Review Letters

Andreev Reflection in an *s*-Type Superconductor Proximized 3D Topological Insulator

E. S. Tikhonov,[1,2] D. V. Shovkun,[1,2] M. Snelder,[3] M. P. Stehno,[3] Y. Huang,[4] M. S. Golden,[4] A. A. Golubov,[2,3] A. Brinkman,[3] and V. S. Khrapai[1,2]

[1]*Institute of Solid State Physics, Russian Academy of Sciences, 142432 Chernogolovka, Russian Federation*
[2]*Moscow Institute of Physics and Technology, Dolgoprudny, 141700 Russian Federation*
[3]*MESA+ Institute for Nanotechnology, University of Twente, 7500 AE Enschede, The Netherlands*
[4]*Van der Waals—Zeeman Institute, University of Amsterdam, 1098 XH Amsterdam, The Netherlands*

(Received 31 March 2016; revised manuscript received 21 June 2016; published 28 September 2016)

We investigate transport and shot noise in lateral normal-metal–3D topological-insulator–superconductor contacts, where the 3D topological insulator (TI) is based on Bi. In the normal state, the devices are in the elastic diffusive transport regime, as demonstrated by a nearly universal value of the shot noise Fano factor $F_N \approx 1/3$ in magnetic field and in a reference normal-metal contact. In the absence of magnetic field, we identify the Andreev reflection (AR) regime, which gives rise to the effective charge doubling in shot noise measurements. Surprisingly, the Fano factor $F_{\mathrm{AR}} \approx 0.22 \pm 0.02$ is considerably reduced in the AR regime compared to F_N, in contrast to previous AR experiments in normal metals and semiconductors. We suggest that this effect is related to a finite thermal conduction of the proximized, superconducting TI owing to a residual density of states at low energies.

DOI: 10.1103/PhysRevLett.117.147001

The surface state of a three-dimensional topological insulator (3D TI) is a unique example of a spin-orbit-coupled and symmetry-protected conductor [1]. Similar to graphene, with 3D TIs the surface electronic states are massless Dirac fermions. Unlike graphene, however, a single Dirac cone is lacking spin and valley degeneracies. This makes the 3D TI an intriguing candidate for the realization of a solid-state two-dimensional topological superconductor [2]. As originally proposed by Fu and Kane [3], *p*-wave-like superconducting correlations are expected to emerge via proximity coupling the 3D TI to a conventional *s*-type superconductor (*S*). This gives rise to symmetry-protected Majorana zero modes bound at the vortices or at the boundaries of various hybrid structures [4,5]. Emerging zero modes are predicted to have a strong impact on the low-energy physics, modifying Andreev reflection (AR) at the interface with a normal metal [6] affecting the edge conductance distribution [7], noise [8], and thermal transport [9,10].

Proximity-induced superconductivity has been demonstrated in 3D TIs based on Bi [11–17] and HgTe [18,19] with the reported values of the induced gap on the order of a few 100 μeV. Similar gap values were recently observed via Andreev spectroscopy [20] in quaternary Bi-Sb-Te-Se compound established as a 3D TI with negligible contribution of the bulk conduction [21,22]. In spite of these advances, the microscopic nature of the proximity-induced gap in Bi-based 3D TIs remains largely unexplored. This particularly concerns the statistics of the transmission eigenvalue distribution in short junctions and the role of possible in-gap states. On this route, valuable information, often hidden in transport, can be obtained via measurements of the nonequilibrium current fluctuations—the shot noise [23]. Relevant for the AR, prominent examples include unusual shot noise behavior at the interface between a normal metal and superconductors with other than *s*-type order parameter symmetry [24,25] and, more recently, shot noise detection of the thermal and charge transport via Majorana zero modes [9,10,26].

Here, we investigate the AR in lateral *N*-TI-*S* contacts defined on thin flakes of 3D TI $Bi_{1.5}Sb_{0.5}Te_{1.7}Se_{1.3}$. By measuring the shot noise, we identify the effective charge (q) and the Fano factor (F), which characterize the random process of charge transport [23]. We demonstrate diffusive normal transport with $q = e$ and $F_N \simeq 1/3$ in *N*-TI-*S* contacts that are subjected to magnetic fields (B) that are large enough to suppresses superconductivity and in the reference *N*-TI-*N* contact. In zero magnetic field, the AR regime is characterized by the doubling of the effective charge $q = 2e$ and $F_{\mathrm{AR}} = 0.22 \pm 0.02$. Our main observation that $F_{\mathrm{AR}} < F_N$ is unusual compared with experiments in normal-metal- [27] and semiconductor–based [28] *N*-*S* contacts.

Our devices are based on thin mechanically exfoliated flakes of a 3D TI $Bi_{1.5}Sb_{0.5}Te_{1.7}Se_{1.3}$ crystal placed on a Si/SiO_2 substrate. The size of the flakes is ~2–4 μm with a thickness in the range of 80–200 nm. The typical carrier densities and mean free paths in our devices are on the order of 10^{13} cm^{-2} and $l \sim 10$ nm, respectively. A scanning electron micrograph of a typical *N*-TI-*S* device is shown in Fig. 1 (on the rhs). In a two-step *e*-beam lithography process, we pattern the *N* electrode (60 nm of sputter-deposited Au with a 3 nm Ti sticking layer) followed by the *S* electrode (a 80 nm thick Nb film with a

critical temperature of 8.4 K). A 15 s long 300 V rf Ar plasma etch was carried out *in situ* prior to the sputter deposition in order to improve the quality of the interfaces. The width of the electrodes is about 300 nm, and the electrode spacing $L \approx 50$ nm is limited by the lithography resolution. These dimensions allowed us to minimize inelastic scattering without compromising a well-defined geometry of the conduction channels. Our experiment is performed in the diffusive limit, $L \gg l$, such that residual inhomogeneities of the current distribution caused by unintentional roughness of the edges of the metallic electrodes and their mutual random misalignment are not important. Altogether, we studied four N-TI-S devices and one N-TI-N device. The measurements were performed in a ^{3}He refrigerator at bath temperatures (T) in the range of 0.6–5 K. Two-terminal differential resistance (R) data were obtained with a lock-in measurement, and a series resistance contribution of wiring was subtracted. The shot noise was measured within an ~5 MHz frequency band around a 18 MHz center frequency of a resonant tank circuit. The tank circuit consisted of a 3.2 μH hand-wound inductor, the 25 pF capacitance of a coaxial cable, and a load resistance of 10 kΩ. The setup was calibrated by means of Johnson-Nyquist thermometry. Where used, the magnetic field was directed perpendicular to the TI plane.

In Fig. 1, we plot the linear response resistances R as a function of the applied magnetic field B for the N-TI-S devices (s1–s4) and the reference N-TI-N device (n) at $T \approx 0.6$ K. Both the zero field resistance $R(B = 0)$ and the relative magnetoresistance vary appreciably among the devices. Nevertheless, in all cases, a sizable positive magnetoresistance is found, reminiscent of a B-driven suppression of the weak antilocalization quantum correction in a strongly spin-orbit-coupled system [29,30]. The absence of a distinct difference between the N-TI-S and the N-TI-N data is a strong indication that the device resistance is dominated by the disordered 3D TI surface. This conjecture is confirmed by the shot noise experiments below.

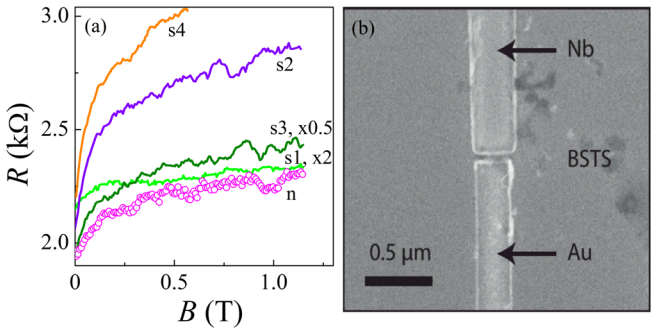

FIG. 1. Magnetotransport data and sample layout. Left: Linear response resistances as functions of perpendicular magnetic field for the normal-metal–TI–normal-metal (N-TI-N) device (n, symbols) and normal-metal–TI–superconductor (N-TI-S) devices (s1–s4, lines) measured at $T = 0.6$ K. For the devices s1 and s3, the data were multiplied by factors of 2 and 0.5, respectively. Right: A scanning electron micrograph of the inner part of one of our N-TI-S devices.

Diffusive transport behavior ($L \gg l$) is showcased in Fig. 2 (left axis), where we plot the shot noise spectral density S_I (symbols) as a function of the bias voltage V for the N-TI-N device at $T \approx 0.6$ K. The $B = 0$ and $B \approx 1.2$ T data are shown with dots and crosses, respectively. In both cases, we observe conventional shot noise behavior of a metallic diffusive conductor for $|V| \leq 1.5$ mV. Here, S_I crosses over from the equilibrium Johnson-Nyquist value of $4k_BT/R$ at $V = 0$ to the linear dependence $S_I = 2qFI$ at $|V| \gg k_BT/q$, where I is the bias current and F is the Fano factor. This crossover is described by the standard noise expression [23]

$$S_I = \frac{4k_BT}{R}(1 - F + F\xi\coth\xi), \qquad \xi \equiv \frac{|qV|}{2k_BT}, \quad (1)$$

where q is the effective charge of the carriers, and a linear dependence $I = V/R$ is assumed. The corresponding best fit with $q = e$ and $F \approx 0.33$ is shown ($B = 0$, dashed line). These data are consistent with the universal (i.e., geometry-independent) value $F = 1/3$ found for metallic conductors in the elastic diffusive regime of transport [31,32] but has not been reported in the TI surface states previously. Above $|V| \approx 1.5$ mV, the experimental data deviate from the theoretical curve, as inelastic electron-phonon scattering processes come into play and start to suppress the noise [31].

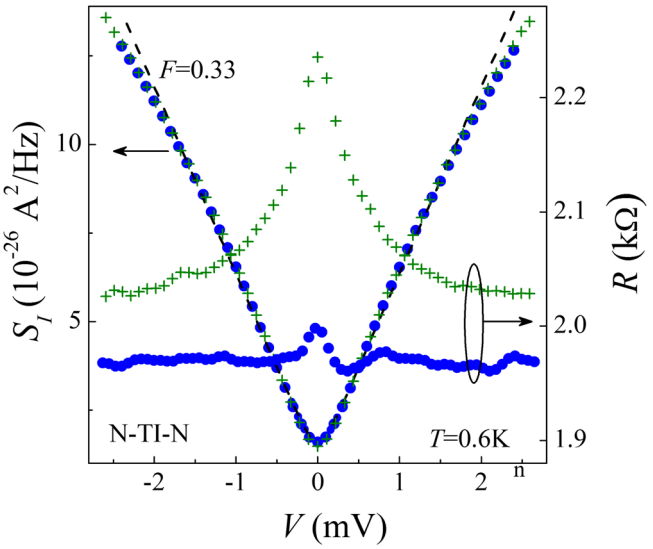

FIG. 2. Shot noise and transport in the reference N-TI-N device. Left axis: Bias voltage dependence of the measured shot noise spectral density at $B = 0$ T (circles) and $B = 1.2$ T (crosses). The fit using Eq. (1) with $F = 0.33$ is shown by the dashed line. Right axis: Differential resistance $R = (dV/dI)$ as a function of the bias voltage across the device at $B = 0$ (circles) and $B = 1.2$ T (crosses).

We conclude our discussion of transport data in the N-TI-N device by analyzing the differential resistance (dV/dI) plotted in Fig. 2 (right axis). The variations in the differential resistance are small, which justifies our use of Eq. (1) and ensures accuracy within a few percent of the extracted value for F. Notably, while (dV/dI) exhibits a sizeable zero bias peak in magnetic field (about 10% in magnitude; upper curve), a much smaller peak is observed for $B = 0$ (lower curve). This indicates the presence of an additional quantum correction to the conductance due to electron-electron interaction [(EEI), Altshuler-Aronov effect], which is also supported by the observation of a weakly insulating temperature dependence in zero magnetic field. At $B = 0$, the corrections owing to the EEI and the weak antilocalization are comparable in magnitude and roughly cancel each other in present devices [33].

In the following, we discuss the Andreev reflection in N-TI-S devices. In Fig. 3(a), we plot typical differential resistance as a function of bias voltage V in zero field and for finite B. The main features of Fig. 3(a), namely, the smaller and narrower zero bias peaks in $B = 0$ compared to the case of finite B field, are similar to those in the N-TI-N device; cf. Fig. 2. Such similarity persists up to 10 mV, which is the highest bias voltage we applied; see the Supplemental Material [34] for more details. This further suggests that the zero bias resistance peaks are intrinsic to the 3D TI surface state. The lack of AR-related resistance features allows us to estimate a transparency of the lateral interface between the normal and strongly proximized TI [Fig. 4(b)], $\Gamma > \sqrt{l/L} \sim 0.4$, which is sufficiently high for negligible reflectionless tunneling in diffusive N-S junctions [42–44].

In Fig. 3(b), we plot the bias dependence of S_I for samples s1–s3 at $T \approx 0.6$ K and $B = 0$. The crossover between the Johnson-Nyquist and the shot noise regime is also observed here. Yet, a closer look reveals two important distinctions compared to the N-TI-N device. First, the shot noise is stronger in N-TI-S devices, and, second, the crossover region is narrower than Eq. (1) predicts. This is demonstrated by the solid line fits in Fig. 3(b), where we used $q = e$ and different Fano factors $0.38 \leq F \leq 0.48$ fixed by the slope of each data set in the shot noise regime. We attribute the narrowing of the crossover region to the impact of the AR at the TI-S interface, which gives rise to doubling of the effective charge in diffusive N-S contacts [27,45]. Using the analog of Eq. (1) with effective charge [46,47] $q = 2e$ and, correspondingly, twice smaller Fano factors ($0.19 \leq F \leq 0.24$), we obtained nearly perfect fits [see the dashed lines in Fig. 3(b)]. As shown in Fig. 3(c), the normal diffusive transport regime is restored for sufficiently high magnetic fields $B \gtrsim 1$ T, as expected. Here, the data in all three devices (symbols) are again consistent with $q = e$ and $0.31 \leq F \leq 0.36$ (solid lines), very much like in the N-TI-N contact; cf. Fig. 2. By contrast, the $q = 2e$ fits fail to account for the bias dependence of S_I in magnetic field; see the dashed lines in Fig. 3(c).

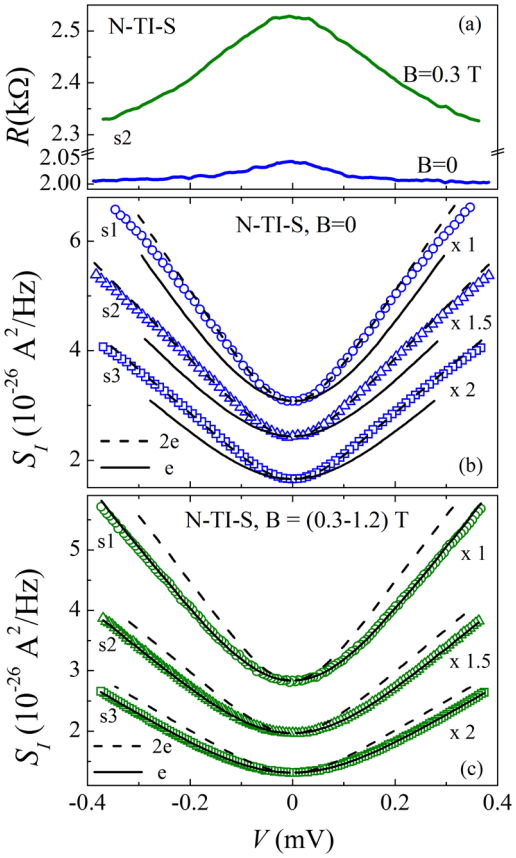

FIG. 3. Transport and shot noise in N-TI-S devices. (a) Typical bias voltage dependence of the differential resistance measured in a N-TI-S device s2 at $B = 0$ T and $B = 0.3$ T. (b) Measured shot noise spectral density (symbols) as a function of the bias voltage across the device in zero magnetic field. The fits using Eq. (1) with $q = e$, $0.38 \leq F \leq 0.48$ and $q = 2e$, $0.19 \leq F \leq 0.24$ are shown by solid and dashed lines, respectively. The data sets are multiplied by 1, 1.5, and 2, respectively, from top to bottom. (c) $S_I(V)$ (symbols) in perpendicular magnetic field. The fits with $q = e$, $0.31 \leq F \leq 0.36$ and $q = 2e$, $0.15 \leq F \leq 0.18$ are shown by solid and dashed lines, respectively. Different traces correspond to devices s1, s2, and s3 as marked in the figure.

In Fig. 4(a), we plot the noise temperature $T_N \equiv S_I R/4k_B$ as a function of V in device s3 in the mV range. The $B = 0$ trace (thick solid line) deviates from the $q = 2e$ fit (thin dotted line) at $|V| \approx 0.35$ mV as marked by the arrows. Remarkably, above this point, the behavior of $T_N(V)$ coincides with that of the normal transport regime. To demonstrate this, we plot the trace for applied magnetic field ($B = 1.16$ T, thick dashed line) and the $q = e$ fit (thin dotted line), both offset vertically. Here, as in previous studies [28,48], the data manifest a finite bias $2e \rightarrow e$ transition from the AR-dominated subgap transport to the normal transport regime above the gap [49]. The corresponding induced proximity gap (on the surface of the 3D TI underneath the Nb film) equals approximately $\Delta'_{\mathrm{STI}} \approx 0.35$ meV in device s3. In the same manner, we obtained proximity gaps of $\Delta'_{\mathrm{STI}} \sim 0.25$–$0.3$ meV in

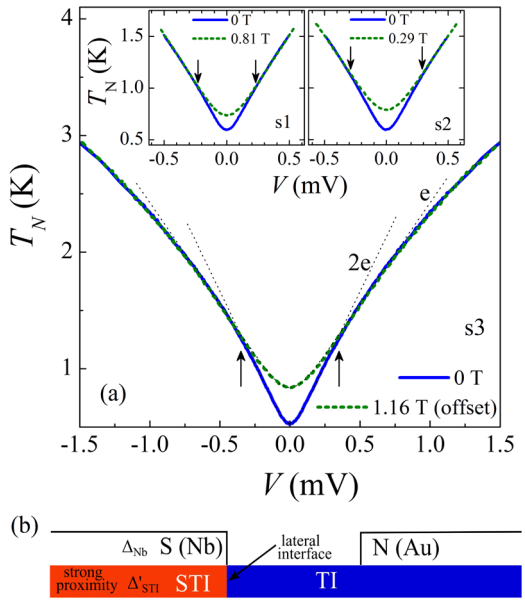

FIG. 4. Finite bias $2e \to e$ transition and proximity gap. (a) Body: Measured noise temperature vs V in the AR regime (thick solid line) and in the normal transport regime (thick dashed line offset by 0.32 K) in device s3, $T \approx 0.53$ K. Corresponding $2e$ and e fits are shown by thin dotted lines. The $2e \to e$ transition at the edge of the proximity gap $|V| \approx 0.35$ mV is marked by arrows. Note that thick solid and dashed lines closely coincide up to $|V| \approx 5$ mV, which is not shown in figure. Insets: Similar $2e \to e$ transitions in the devices s1 and s2. (b) Proximity effect in a lateral N-TI-S junction. A superconducting gap Δ'_{STI} opens in a strongly proximized TI (STI) beneath the Nb film. Lateral interface between the STI and normal TI relevant for noise and transport in the AR regime is indicated by an arrow.

devices s1 and s2 [see insets in Fig. 4(a)]. These values are significantly smaller than the pairing potential in the niobium electrode $\Delta_{Nb} \approx 1.3$ meV, which is estimated from a measurement of the critical temperature. It is worth pointing out that a similar suppression is found for the characteristic energy of the Josephson coupling in Josephson junctions with TI weak links. Typical values for the product of critical current and normal state resistance ($I_C R_N$) are $0.01–0.2\Delta_{Nb}/e$; see Table I in Ref. [17]. The reduction is attributed to an interface barrier between the superconducting electrode and the TI material. Disorder effects must also be considered [50,51].

The observation of charge doubling and a $2e \to e$ transition in Figs. 3(b) and 4(a) is clear evidence of AR in $B = 0$. Surprisingly, the Fano factor in the AR regime $F_{AR} = 0.22 \pm 0.02$ is considerably smaller than the universal value $F_N = 1/3$ attained in the normal transport regime in magnetic field [Fig. 3(c)] and in the reference N-TI-N device (Fig. 2). Similar behavior is found in all three devices with device resistances ranging from 1 to 4 kΩ. This is our main observation. It is in sharp contrast to measurements in normal-metal- [27] and semiconductor-based [28] N-S contacts. In the former case, $F_{AR} = F_N = 1/3$, as expected for the universal eigenvalue distribution of metallic diffusive conductors [42], while in the latter case, $F_{AR} > F_N$ was found [52].

The observed reduction of the shot noise in the AR regime can be understood intuitively in the framework of heat transport as follows; see Ref. [53]. In the case of perfect AR, the heat transport across the N-S interface vanishes, which results in exact shot noise doubling for the N-S contact. Finite heat conduction in the S lead can reduce the shot noise below this limit. In particular, disorder effects may result in a finite, residual density of states in the STI below the Nb contact. This opens a parallel transport channel for heat conduction by quasiparticles, thus, reducing AR. Additionally, we consider the nontrivial gap structure of the induced proximity effect in the STI. It has been shown in Refs. [24,25] that in-gap Andreev bound states which are formed in junctions with p- and d-wave superconductors due to a phase shift in the order parameter between different crystal directions alter the junction transmission and reduce the shot noise. We would like to mention that similar scenario has been proposed for normal-metal–ferromagnetic-insulator–superconductor structures where a finite magnetic polarization is induced by the ferromagnetic insulator and chiral Majorana zero mode forms [4].

In summary, we investigated the shot noise in N-TI-S contacts defined on thin flakes of 3D TI $Bi_{1.5}Sb_{0.5}Te_{1.7}Se_{1.3}$. We identified both the carrier charge q and the Fano factor characterizing the randomness of the discrete charge transport. In the normal state, the elastic diffusive transport regime is evidenced via charge $q = e$ and nearly universal Fano factor $F_N \approx 1/3$ in N-TI-S contacts in magnetic field and in a reference N-TI-N device. In the AR regime in $B = 0$, the effective charge doubles $q = 2e$, whereas the Fano factor is considerably reduced $F_{AR} \approx 0.22 \pm 0.02$. Our main observation of $F_{AR} < F_N$ is in contrast with the available shot noise measurements in normal-metal- and semiconductor-based devices [27,28]. Possible presence of low-energy Andreev bound states or in-gap states in the superconductor proximized 3D TI qualitatively explains our results.

We thank K. E. Nagaev and Y. Tanaka for fruitful discussions. This work was supported in part by the Russian Academy of Sciences, the Ministry of Education and Science of the Russian Federation Grant No. 14Y.26.31.0007, the RFBR Grants No. 16-32-00869 and No. 15-02-04285, and the Russian Science Foundation Project No. 15-12-30030. Part of this work was funded by the Foundation for Fundamental Research on Matter, which is part of the Netherlands Organisation for Scientific Research, and the European Research Council.

[1] M. Z. Hasan and C. L. Kane, Rev. Mod. Phys. **82**, 3045 (2010).
[2] X.-L. Qi and S.-C. Zhang, Rev. Mod. Phys. **83**, 1057 (2011).
[3] L. Fu and C. L. Kane, Phys. Rev. Lett. **100**, 096407 (2008).

[4] Y. Tanaka, T. Yokoyama, and N. Nagaosa, Phys. Rev. Lett. **103**, 107002 (2009).
[5] J. Alicea, Rep. Prog. Phys. **75**, 076501 (2012).
[6] C. W. J. Beenakker, J. P. Dahlhaus, M. Wimmer, and A. R. Akhmerov, Phys. Rev. B **83**, 085413 (2011).
[7] C. W. J. Beenakker, Rev. Mod. Phys. **87**, 1037 (2015).
[8] C. J. Bolech and E. Demler, Phys. Rev. Lett. **98**, 237002 (2007).
[9] A. R. Akhmerov, J. P. Dahlhaus, F. Hassler, M. Wimmer, and C. W. J. Beenakker, Phys. Rev. Lett. **106**, 057001 (2011).
[10] M. Diez, I. C. Fulga, D. I. Pikulin, J. Tworzydło, and C. W. J. Beenakker, New J. Phys. **16**, 063049 (2014).
[11] D. Zhang, J. Wang, A. M. DaSilva, J. S. Lee, H. R. Gutierrez, M. H. W. Chan, J. Jain, and N. Samarth, Phys. Rev. B **84**, 165120 (2011).
[12] B. Sacépé, J. B. Oostinga, J. Li, A. Ubaldini, N. J. Couto, E. Giannini, and A. F. Morpurgo, Nat. Commun. **2**, 575 (2011).
[13] M. Veldhorst, M. Snelder, M. Hoek, T. Gang, V. K. Guduru, X. L. Wang, U. Zeitler, W. G. van der Wiel, A. A. Golubov, H. Hilgenkamp, and A. Brinkman, Nat. Mater. **11**, 417 (2012).
[14] M.-X. Wang, C. Liu, J.-P. Xu, F. Yang, L. Miao, M.-Y. Yao, C. L. Gao, C. Shen, X. Ma, X. Chen, Z.-A. Xu, Y. Liu, S.-C. Zhang, D. Qian, J.-F. Jia, and Q.-K. Xue, Science **336**, 52 (2012).
[15] J. R. Williams, A. J. Bestwick, P. Gallagher, S. S. Hong, Y. Cui, A. S. Bleich, J. G. Analytis, I. R. Fisher, and D. Goldhaber-Gordon, Phys. Rev. Lett. **109**, 056803 (2012).
[16] S. Cho, B. Dellabetta, A. Yang, J. Schneeloch, Z. Xu, T. Valla, G. Gu, M. J. Gilbert, and N. Mason, Nat. Commun. **4**, 1689 (2013).
[17] L. Galletti, S. Charpentier, M. Iavarone, P. Lucignano, D. Massarotti, R. Arpaia, Y. Suzuki, K. Kadowaki, T. Bauch, A. Tagliacozzo, F. Tafuri, and F. Lombardi, Phys. Rev. B **89**, 134512 (2014).
[18] J. B. Oostinga, L. Maier, P. Schüffelgen, D. Knott, C. Ames, C. Brüne, G. Tkachov, H. Buhmann, and L. W. Molenkamp, Phys. Rev. X **3**, 021007 (2013).
[19] J. Wiedenmann, E. Bocquillon, R. S. Deacon, S. Hartinger, O. Herrmann, T. M. Klapwijk, L. Maier, C. Ames, C. Brüne, C. Gould, A. Oiwa, K. Ishibashi, S. Tarucha, H. Buhmann, and L. W. Molenkamp, Nat. Commun. **7**, 10303 (2016).
[20] M. Snelder, M. P. Stehno, A. A. Golubov, C. G. Molenaar, T. Scholten, D. Wu, Y. K. Huang, W. G. van der Wiel, M. S. Golden, and A. Brinkman, arXiv:1506.05923.
[21] Z. Ren, A. A. Taskin, S. Sasaki, K. Segawa, and Y. Ando, Phys. Rev. B **84**, 165311 (2011).
[22] Y. Pan, D. Wu, J. R. Angevaare, H. Luigjes, E. Frantzeskakis, N. de Jong, E. van Heumen, T. V. Bay, B. Zwartsenberg, Y. K. Huang, M. Snelder, A. Brinkman, M. S. Golden, and A. de Visser, New J. Phys. **16**, 123035 (2014).
[23] Y. Blanter and M. Büttiker, Phys. Rep. **336**, 1 (2000).
[24] J.-X. Zhu and C. S. Ting, Phys. Rev. B **59**, R14165 (1999).
[25] Y. Tanaka, T. Asai, N. Yoshida, J. Inoue, and S. Kashiwaya, Phys. Rev. B **61**, R11902 (2000).
[26] A. Zazunov, R. Egger, and A. Levy Yeyati, Phys. Rev. B **94**, 014502 (2016).
[27] A. A. Kozhevnikov, R. J. Schoelkopf, and D. E. Prober, Phys. Rev. Lett. **84**, 3398 (2000).
[28] B.-R. Choi, A. E. Hansen, T. Kontos, C. Hoffmann, S. Oberholzer, W. Belzig, C. Schönenberger, T. Akazaki, and H. Takayanagi, Phys. Rev. B **72**, 024501 (2005).
[29] S. Hikami, A. I. Larkin, and Y. Nagaoka, Prog. Theor. Phys. **63**, 707 (1980).
[30] B. L. Altshuler, D. Khmel'nitzkii, A. I. Larkin, and P. A. Lee, Phys. Rev. B **22**, 5142 (1980).
[31] K. E. Nagaev, Phys. Lett. A **169**, 103 (1992).
[32] C. W. J. Beenakker and M. Büttiker, Phys. Rev. B **46**, 1889 (1992).
[33] H.-Z. Lu and S.-Q. Shen, Phys. Rev. Lett. **112**, 146601 (2014).
[34] See the Supplemental Material at http://link.aps.org/supplemental/10.1103/PhysRevLett.117.147001, which includes Refs. [35–41], for the additional transport and noise data.
[35] S. S. Kubakaddi, Phys. Rev. B **79**, 075417 (2009).
[36] J. K. Viljas and T. T. Heikkilä, Phys. Rev. B **81**, 245404 (2010).
[37] A. C. Betz, F. Vialla, D. Brunel, C. Voisin, M. Picher, A. Cavanna, A. Madouri, G. Fève, J.-M. Berroir, B. Plaçais, and E. Pallecchi, Phys. Rev. Lett. **109**, 056805 (2012).
[38] A. M. R. Baker, J. A. Alexander-Webber, T. Altebaeumer, and R. J. Nicholas, Phys. Rev. B **85**, 115403 (2012).
[39] K. C. Fong and K. C. Schwab, Phys. Rev. X **2**, 031006 (2012).
[40] A. Sergeev and V. Mitin, Phys. Rev. B **61**, 6041 (2000).
[41] Y. H. Wang, D. Hsieh, E. J. Sie, H. Steinberg, D. R. Gardner, Y. S. Lee, P. Jarillo-Herrero, and N. Gedik, Phys. Rev. Lett. **109**, 127401 (2012).
[42] C. W. J. Beenakker, Rev. Mod. Phys. **69**, 731 (1997).
[43] A. Volkov, A. Zaitsev, and T. Klapwijk, Physica C (Amsterdam) **210C**, 21 (1993).
[44] F. W. J. Hekking and Y. V. Nazarov, Phys. Rev. Lett. **71**, 1625 (1993).
[45] X. Jehl, M. Sanquer, R. Calemczuk, and D. Mailly, Nature (London) **405**, 50 (2000).
[46] V. A. Khlus, Sov. Phys. JETP **66**, 1243 (1987).
[47] T. Martin, Phys. Lett. A **220**, 137 (1996).
[48] A. Das, Y. Ronen, M. Heiblum, D. Mahalu, A. V. Kretinin, and H. Shtrikman, Nat. Commun. **3**, 1165 (2012).
[49] At even higher bias, $|V| > 0.8$ mV, the noise is influenced by electron-phonon relaxation; see the Supplemental Material [34] for more details.
[50] J. D. Sau, R. M. Lutchyn, S. Tewari, and S. Das Sarma, Phys. Rev. B **82**, 094522 (2010).
[51] A. C. Potter and P. A. Lee, Phys. Rev. B **83**, 184520 (2011).
[52] Note that Ref. [28] defined the Fano factor as $F = S_I/2eI$ in both the normal and the AR regimes, which resulted in $F_{\mathrm{AR}}/F_N > 2$.
[53] K. E. Nagaev and M. Büttiker, Phys. Rev. B **63**, 081301 (2001).